ACS APPLIED NANO MATERIALS

www.acsanm.org Article

Anisotropically Enhanced Second Harmonic Generation in a WS_2 Nanoparticle Driven by Optical Resonances

Tianxiang Yu,[#] Mingcheng Panmai,[#] Shulei Li, Shimei Liu, Yuheng Mao, Lidan Zhou, and Sheng Lan*

Cite This: *ACS Appl. Nano Mater.* 2024, 7, 726−735 Read Online

ACCESS | Metrics & More | Article Recommendations | Supporting Information

ABSTRACT: Transition metal dichalcogenides (TMDCs) have attracted great interest due to their excellent electronic and optical properties. Although much attention has been paid to TMDC monolayers, the high refractive index of bulk TMDCs in the lossless region implies potential applications of TMDC nanoparticles/nanostructures in the fields of nanophotonics and nonlinear optics. In this work, the second harmonic generation (SHG) in WS_2 nanoparticles with different geometrical symmetries is investigated both numerically and experimentally. It is revealed that such a WS_2 nanoparticle supports electric dipole (ED) mode, anapole mode, and whispering gallery mode (WGM) in which the SHG is enhanced. It is found that the SHG from a WS_2 nanoparticle with C_2 symmetry exhibits a strong dependence on the polarization of the excitation laser light around the ED resonance. Interestingly, it is observed that the SHG intensities at the two polarization angles perpendicular to each other (θ = 0° and θ = 90°) become equal at the ED resonance. On the short-wavelength side of the ED resonance, the SHG intensity at θ = 0° is smaller than that at θ = 90°. The situation is reversed on the long-wavelength side. The strongest SHG is achieved at the anapole resonance for θ = 0° and at the WGM resonance for θ = 90°. The polarization-dependent ED resonance manifested in the scattering spectra of the WS_2 nanoparticle is responsible for this behavior. In a WS_2 nanodisk, the SHG becomes insensitive to the polarization of the excitation laser light. It is shown that the SHG intensity from a WS_2 nanoparticle is much larger than that from a WS_2 monolayer, with an enhancement factor of up to ~30. Our findings suggest a way to enhance and manipulate the second-order nonlinear optical responses of TMDC nanoparticles and lay a foundation for the realization of TMDC-based photonic devices.

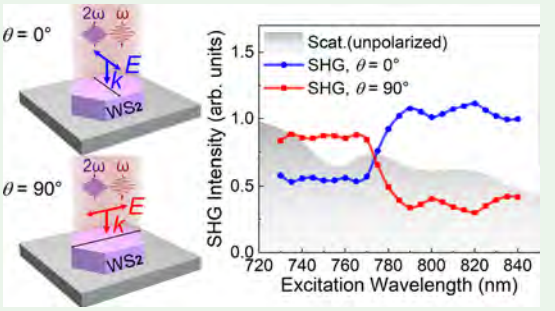

KEYWORDS: *WS_2 nanoparticle, scattering, electric dipole, anapole, whispering gallery mode, second harmonic generation*

INTRODUCTION

As a core research in nonlinear optics, second harmonic generation (SHG) has been widely used in short-wavelength coherent light sources, ultrafast optical modulation, biosensing, quantum information processing, etc.[1−5] Limited by the symmetry of the atomic structure, however, SHG is not supported in centrosymmetric materials. Based on the dipole approximation theory, the second-order nonlinear polarizability vanishes (i.e., $\chi^{(2)} = 0$) in such materials, implying that SHG is forbidden.[6] In order to overcome this limitation, symmetry breaking is generally employed to realize SHG in centrosymmetric materials. From the microscopic point of view, the discontinuity of atoms on the surface or edge of the structure automatically breaks the symmetry of the atomic structure, resulting in the polarization source.[7,8] On the other hand, symmetry breaking can also be achieved by designing an asymmetric structure.[9,10] Following these strategies, the enhancement and manipulation of SHG in metallic nanoparticles and nanostructures have received intensive and extensive studies in the last two decades. In comparison, less attention has been paid to dielectric nanoparticles and nanostructures made of centrosymmetric materials.

In recent years, dielectric nanomaterials and nanostructures with high refractive indexes, such as nanoparticles,[11] nanodisks,[12] nanowires,[13] and metasurfaces,[14] have become the focus of many studies for the enhancement and manipulation of SHG because significant electric field enhancement can be achieved at the optical resonances supported by these nanostructures.[15,16] Since the optical modes excited in such dielectric nanomaterials usually exhibit nonuniform electric field distributions over the constituent atoms, SHG can also be realized in dielectric materials with centrosymmetry. The enhancement of the electric field in combination with the second-order nonlinear polarization source implies that one can achieve enhanced SHG at the optical resonances of dielectric nanoparticles.

Received: October 10, 2023
Revised: November 30, 2023
Accepted: November 30, 2023
Published: December 14, 2023

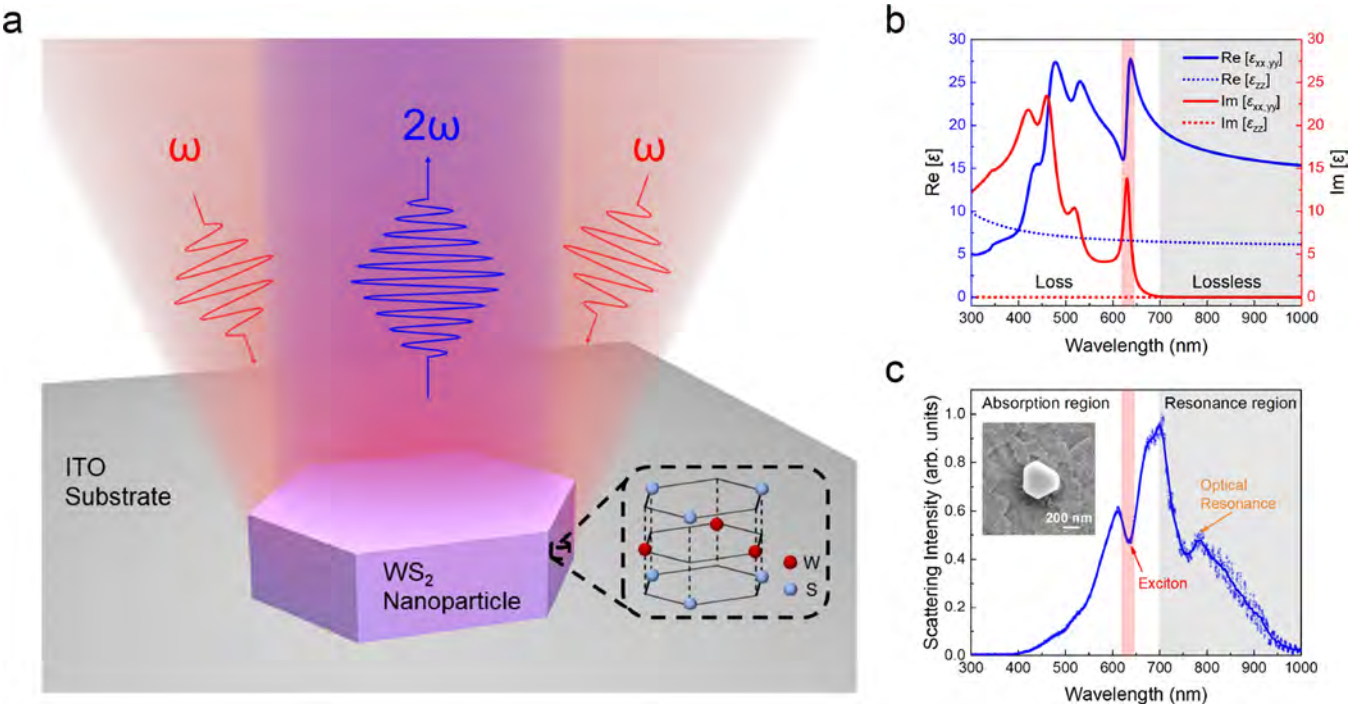

Figure 1. (a) Schematic showing the SHG process from a WS_2 nanoparticle excited by femtosecond laser light. (b) Permittivity of bulk WS_2. The lossless region is marked by gray color. (c) Scattering spectrum of a typical WS_2 nanoparticle. The SEM image of the WS_2 nanoparticle is shown in the inset.

Recently, transition metal dichalcogenides (TMDCs) have attracted great interest in nanophotonics due to their unique optical properties. Most TMDCs exhibit large and anisotropic permittivities.[17−19] In the near-infrared spectral range where the optical loss of most TMDCs is negligible, some TMDCs (e.g., MoS_2 and WS_2) possess permittivities larger than those of silicon (Si), germanium (Ge), and III−V compound semiconductors (e.g., GaAs). Moreover, these TMDCs exhibit significant exciton effects at room temperature,[20−22] which dramatically enhance the light−matter interaction.[23] These advantages make TMDCs potential dielectric materials for building metasurfaces, metamaterials, and photonic devices, which has become a research hotspot in the field of nanophotonics. However, SHG in bulk TMDCs with centrosymmetry (e.g., MoS_2 and WS_2) is negligible.[6,24] For TMDCs with centrosymmetry, SHG is observed only in TMDCs with odd layers and its intensity decreases rapidly with an increasing layer number.[25−27] So far, two strategies have usually been employed to enhance the SHG from TMDCs. In the first method, a TMDC monolayer is coupled to a plasmonic or a photonic system supporting optical resonances, such as plasmonic nanostructure,[28,29] optical microcavity,[30−32] plasmonic nanoantenna,[33] etc. In this case, the nonlinear optical responses (e.g., SHG) of the TMDC monolayer are enhanced by the near-field enhancement provided by the optical resonances. In the second method, TMDC nanoparticles or nanostructures supporting directly optical resonances are fabricated to realize simultaneously the symmetry breaking and electric field enhancement. For example, it was shown that WS_2 nanodisks supporting optical resonances can be employed to achieve strong SHG in the visible light spectrum.[34] In addition, lasing from WS_2 nanodisks was also realized at room temperature by exploiting the optical modes supported by WS_2 nanodisks.[35] Enhanced SHG and third harmonic generation can be achieved in metasurfaces made of TMDCs.[36] Quasi-bound states in the continuum with high-quality factors were demonstrated in a MoS_2-based metasurface.[37] These results indicate that the optical modes excited in TMDC nanoparticles can be exploited to break the symmetry of the atomic structure and to realize SHG enhancement.

In this work, we investigated the SHG in WS_2 nanoparticles with different geometrical symmetries, paying attention to the influences of the optical resonances supported by WS_2 nanoparticles on the efficiency of SHG. By exciting WS_2 nanoparticles with tunable femtosecond laser light, we revealed that the SHG of a WS_2 nanoparticle can be enhanced at the electric dipole (ED) resonance, the anapole resonance, and the whispering gallery mode (WGM) resonance of the WS_2 nanoparticle. In addition, we found that the SHG of a WS_2 nanoparticle with C_2 symmetry exhibits a strong dependence on the polarization of the excitation laser light, offering us the opportunity to manipulate the SHG of the WS_2 nanoparticle by simply changing the polarization angle of the excitation laser light. By decomposing the scattering spectrum into Mie resonances, we showed that the polarization-dependent SHG observed in the WS_2 nanoparticle originates from the polarization-dependent ED resonance. We compared the SHG intensity from a WS_2 nanoparticle with that from a WS_2 monolayer and observed an enhancement factor of up to ~30. The numerical analyses and experimental observations provided in this work provide new insights for enhancing and manipulating SHG in TMDC nanoparticles by exploiting the optical modes excited in TMDC nanoparticles. They are helpful for designing TMDC-based photonic devices.

https://doi.org/10.1021/acsanm.3c04844
ACS Appl. Nano Mater. 2024, 7, 726−735

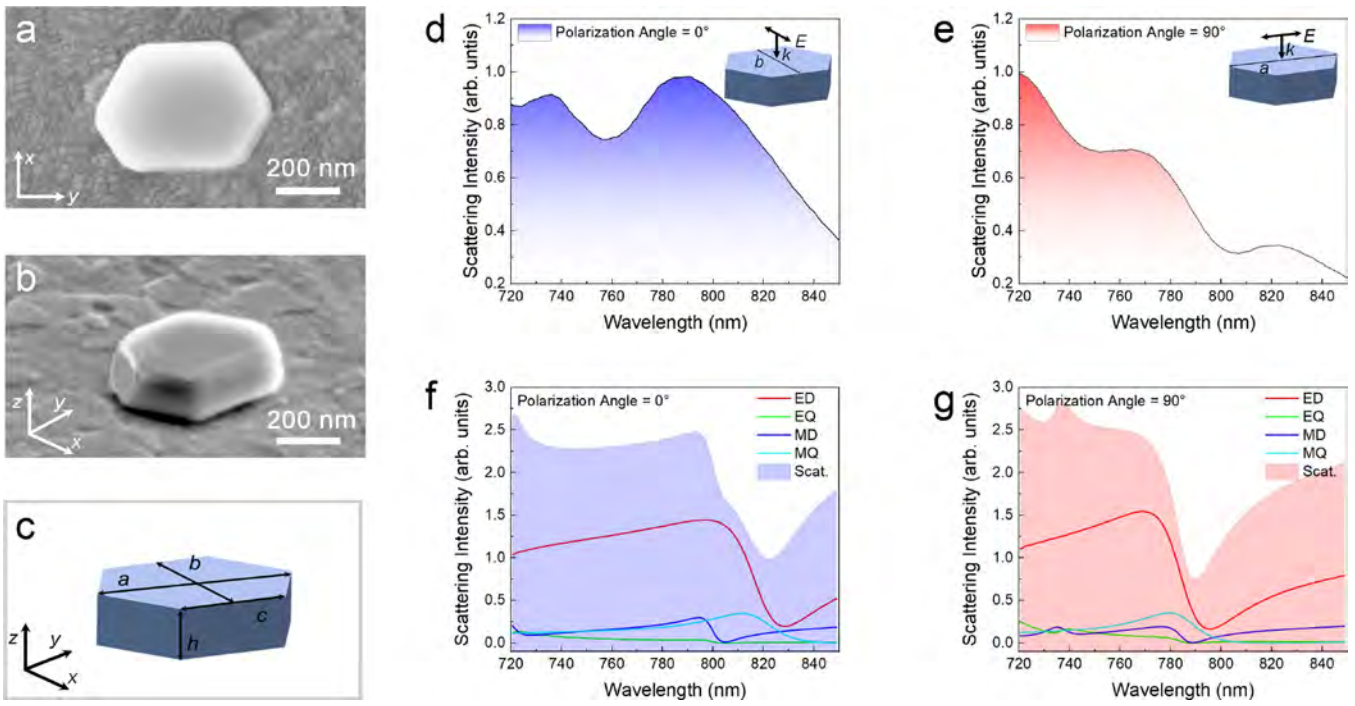

Figure 2. (a, b) SEM images of a hexagonal-prism-like WS_2 nanoparticle taken at a tilt angle of 90° (a) and 45° (b). (c) Schematic showing the geometric structure of a hexagonal-prism-like WS_2 nanoparticle. (d, e) Scattering spectra of the WS_2 nanoparticle measured at polarization angles of $\theta = 0°$ (d) and $\theta = 90°$ (e). In each case, the polarization of the excitation laser light is shown in the inset. (f, g) Simulated scattering spectra of the WS_2 nanoparticle at polarization angles of $\theta = 0°$ (f) and $\theta = 90°$ (g). In each case, the scattering spectrum is decomposed into the contributions of Mie resonances of different orders.

RESULTS AND DISCUSSION

Figure 1a schematically shows the SHG from a hexagonal-prism-like WS_2 nanoparticle excited by femtosecond laser pulses. Such WS_2 nanoparticles were dispersed on a silica (SiO_2) substrate coated with a thin layer of indium tin oxide (ITO). In this work, we chose ITO as the substrate for WS_2 nanoparticles because of its good conductivity. Thus, the morphology characterization based on scanning electron microscopy (SEM) enabled us to find hexagonal-prism-like WS_2 nanoparticles. Since the refractive index of ITO is close to that of SiO_2 and its influence on the scattering properties of a WS_2 nanoparticle is negligible (see the Supporting Information, Figure S1), it has been used as the substrate in the investigation of the SHG from AlGaAs nanoparticles.[15] Based on SEM observation, it was found that most of the WS_2 nanoparticles appeared as hexagonal prisms, although there were also nanoparticles exhibiting other shapes (see the Supporting Information, Figure S2).

Figure 1b shows the permittivity of bulk WS_2 obtained by using spectroscopic ellipsometry.[38] It includes the data of both the in-plane and out-of-plane directions, which is suitable for simulating the optical properties of WS_2 nanoparticles. It is noticed that the imaginary part of the in-plane permittivity (red curve) drops to 0 when the wavelength exceeds ~700 nm. In addition, the real part of the in-plane permittivity (blue curve) is larger than 16. It implies that a WS_2 nanoparticle can support optical resonance in the near-infrared spectral range. In this work, we focus on the nonlinear optical responses of WS_2 nanoparticles in the resonance region (marked by gray color). Since bulk WS_2 is formed by stacking a large number of single layers via the van der Waals force, the optical properties of a WS_2 nanoparticle are also influenced by the out-of-plane permittivity, although its real part is much smaller than that of the in-plane one (see Figure 1b).

Figure 1c shows the scattering spectrum of a typical WS_2 nanoparticle measured by using a dark-field microscope with unpolarized white light. In the absorption region, one can see a scattering valley at $\lambda \approx 630$ nm (marked by the red arrow). It corresponds to the absorption peak (marked by the red shadow) shown in Figure 1b, which originates from the direct bandgap transition of excitons at the K point.[39] In the resonance region, one can identify a low-order Mie resonance (marked by the orange arrow) supported by the WS_2 nanoparticle (for the scattering spectra of more WS_2 nanoparticles, see the Supporting Information, Figure S3).

In this study, we mainly explore the influence of the optical resonances supported by a WS_2 nanoparticle on the SHG of the WS_2 nanoparticle. We chose hexagonal-prism-like WS_2 nanoparticles with an edge length larger than 200 nm so that the low-order Mie resonances supported by WS_2 nanoparticles appeared in the wavelength range of 750−850 nm, which can be easily accessed by conventional femtosecond laser light.

Figure 2a,b shows the morphologies of a targeted WS_2 nanoparticle characterized by SEM, including the top view (Figure 2a) and the side view with a tilt angle of 45° (Figure 2b). The side length and height of the WS_2 nanoparticle, which are used to characterize a hexagonal prism, can be estimated from the SEM images. We also measured the height of the WS_2 nanoparticle by using atomic force microscopy (AFM) (see the Supporting Information, Figure S4). Since most of the WS_2 nanoparticles did not appear as standard hexagonal prisms, we introduce four parameters (a, b, c, and h) to describe the structure of a WS_2 nanoparticle, which represent the long axis, short axis, side length, and height of the WS_2 nanoparticle, respectively, as shown in Figure 2c.

https://doi.org/10.1021/acsanm.3c04844
ACS Appl. Nano Mater. 2024, 7, 726−735

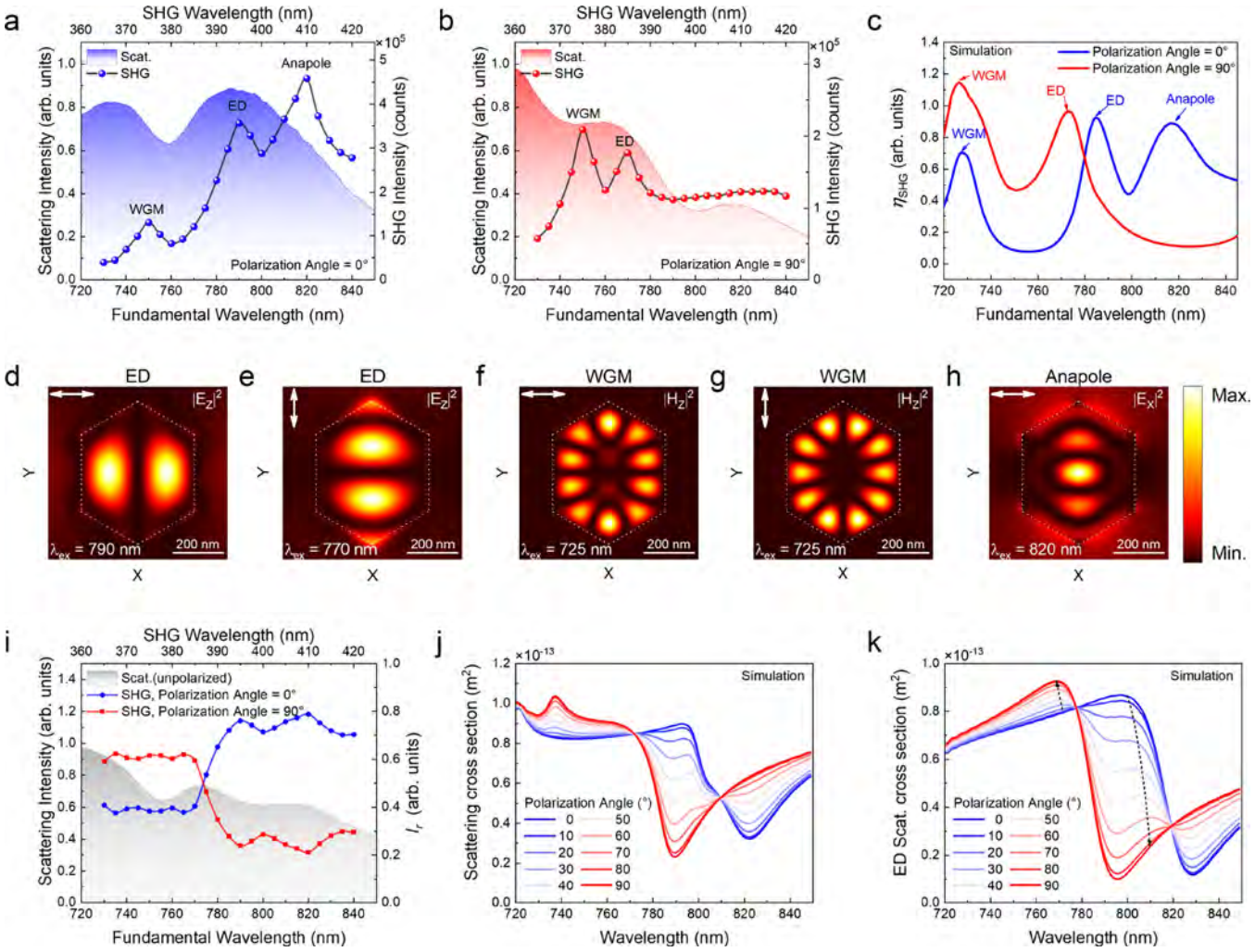

Figure 3. (a, b) Dependence of the SHG intensity on the excitation wavelength observed for the WS_2 nanoparticle at polarization angles of $\theta = 0°$ (a) and $\theta = 90°$ (b). In each case, the scattering spectrum of the WS_2 nanoparticle measured by using white light with the same polarization angle is also provided for reference. (c) Dependence of the SHG efficiency on the excitation wavelength simulated for a WS_2 nanoparticle with the same dimensions at polarization angles of $\theta = 0°$ and $\theta = 90°$. (d–h) Electric/magnetic field distributions calculated at different optical resonances. In each case, the polarization of the excitation light is indicated by an arrow. (i) Dependence of the relative SHG intensity on the excitation wavelength calculated for the WS_2 nanoparticle at polarization angles of $\theta = 0°$ and $\theta = 90°$. The scattering spectrum of the WS_2 nanoparticle illuminated with unpolarized white light is provided for reference. (j) Dependence of the scattering spectrum on increasing polarization angle calculated for the WS_2 nanoparticle with the same dimensions. (k) Dependence of the ED resonance on increasing polarization angle calculated for the WS_2 nanoparticle with the same dimensions.

For the WS_2 nanoparticle shown in Figure 2a,b, the structural parameters were found to be a = 580 nm, b = 444 nm, c = 312 nm, and h = 148 nm. It possesses C_2 symmetry in the $x-y$ plane. Since the femtosecond laser light used to excite the WS_2 nanoparticle is linearly polarized, it is expected that the nonlinear optical responses of the WS_2 nanoparticle are also polarization dependent. For the convenience of discussion, we define the direction along the short axis (b axis) as the polarization angle $\theta = 0°$. Thus, the direction along the long axis (a axis) corresponds to the polarization angle $\theta = 90°$.

In Figure 2d,e, we present the scattering spectra measured for the WS_2 nanoparticle by using white light polarized along the short ($\theta = 0°$) and long axis ($\theta = 90°$), respectively. It is noticed that the scattering peak appears at $\lambda \approx 790$ nm when $\theta = 0°$. For $\theta = 90°$, the scattering peak is blue-shifted to $\lambda \approx 770$ nm. The difference in the scattering peak arises from the difference between the long and short axes. Based on the structural parameters obtained by the SEM observation, we also simulated the scattering spectra of this WS_2 nanoparticle, as shown in Figure 2f,g. It can be seen that the measured scattering spectra agree well with the simulated spectra for wavelengths shorter than 830 nm. The small discrepancies originate mainly from the inaccuracy in the dimension and permittivity of the WS_2 nanoparticle. In the long-wavelength range, the scattering peak in the simulated scattering spectrum was not observed in the measured spectrum due to the low quantum efficiency of the photodetector. In order to understand the physical origin of the scattering peak, the scattering spectrum was decomposed into the contributions of the Mie resonances. It was revealed that the scattering is dominated by the ED resonance in both cases.

Now, we examine the nonlinear optical responses of the WS_2 nanoparticle under the excitation of femtosecond laser pulses. First, the WS_2 nanoparticle was excited by using 800 nm femtosecond laser pulses with different pumping powers (see the Supporting Information, Figure S5). The slope extracted

https://doi.org/10.1021/acsanm.3c04844
ACS Appl. Nano Mater. 2024, 7, 726–735

from the dependence of the SHG intensity on the pumping power plotted in a double logarithmic coordinate was found to be ~1.81, verifying the second-order nonlinear optical effect of SHG. After that, we fixed the polarization angle of the laser light at $\theta = 0°$ or 90° and measured the SHG intensities at different excitation wavelengths. The dependence of the SHG intensity on the excitation wavelength observed at $\theta = 0°$ and $\theta = 90°$ is shown in Figure 3a,b. In both cases, it was found that the SHG of the WS_2 nanoparticle is enhanced at the wavelength corresponding to the scattering peak (i.e., $\lambda_{ex} \approx 790$ nm for $\theta = 0°$ and $\lambda_{ex} \approx 770$ nm for $\theta = 90°$). In both cases, the SHG enhancement was also observed at $\lambda_{ex} \approx 750$ and $\lambda_{ex} \approx 820$ nm. However, the strongest SHG was achieved at $\lambda_{ex} \approx 820$ nm for $\theta = 0°$, while it was obtained at $\lambda_{ex} \approx 750$ nm for $\theta = 90°$.

In order to understand this behavior, we calculated the SHG efficiency of the WS_2 nanoparticle, which can be expressed as follows:

$$\eta_{SHG} = \frac{\int_A \mathbf{S}_{SH} \cdot \mathbf{n} da}{I_0 \times s_A} \quad (1)$$

where $\mathbf{S}_{SH}$ is the Poynting vector of the second harmonic field, $\mathbf{n}$ is the unit vector surrounding the nanoparticle, I_0 is the intensity of the fundamental wave ($I_0 = 1$ GW/cm^2 in the simulation), and s_A is the illumination area of the incident light.

The SHG efficiencies calculated for the WS_2 nanoparticle at $\theta = 0°$ and $\theta = 90°$ are shown in Figure 3c. The calculation results are roughly consistent with the experimental observations shown in Figure 3a,b. However, enhanced SHG efficiency is observed at $\lambda_{ex} \approx 725$ nm in the calculation results, which is slightly different from the measurement results ($\lambda_{ex} \approx 750$ nm). This difference is also induced by the inaccurate dimensions and permittivity of the WS_2 nanoparticle used in the numerical simulations. In order to gain a deep insight into the physical mechanism responsible for the SHG enhancement, we calculated the electromagnetic field distributions at the wavelengths where the SHG is enhanced, as shown in Figure 3d–h. As discussed above, the scattering peak of the WS_2 nanoparticle is dominated by the ED mode. Thus, the SHG enhancement achieved at the scattering peak comes mainly from the electric field enhancement of the ED mode, as shown in Figure 3d,e. Theoretically, SHG is forbidden in bulk WS_2 due to the centrosymmetry of the atomic structure. However, the nonuniform electric field distribution at the optical resonance breaks the symmetry of the electric field exerted on atoms, providing an effective polarization source for SHG. Moreover, the electric field localization at the ED mode enhances the nonlinear optical responses of the WS_2 nanoparticle, leading to the enhanced SHG observed in both the numerical simulation and the experimental observation.

We also examined the magnetic field distributions at $\lambda_{ex} \approx 725$ nm, where the SHG enhancement is observed in both cases (see Figure 3f,g). Apparently, they belong to WGMs supported by the WS_2 nanoparticle. Although the WGMs can be excited in both cases, the field distributions and radiation losses (or quality factors) are different. For $\theta = 0°$, a larger radiation loss leads to weaker SHG enhancement. As compared with the ED and anapole modes, a larger discrepancy is observed between the calculated wavelength and the measured wavelength for the WGM. We think that the larger discrepancy is caused by the deviation of the nanoparticle shape from a perfect hexagonal prism and the inaccuracy of the refractive index of WS_2. Since the electric field of the WGM is mainly distributed on the edges of the nanoparticle, the resonant wavelength of the WGM will be affected by the change in the side length of the hexagonal prism. In addition, the influence of the refractive index on the resonant wavelength of the WGM is also not negligible.

For $\theta = 0°$, it is noticed that the strongest SHG is achieved at $\lambda_{ex} \approx 820$ nm. Based on the electric field distribution calculated at this wavelength (see Figure 3h), it is revealed that the SHG enhancement comes from the anapole mode supported by the WS_2 nanoparticle. The anapole mode originates from interference between the ED and toroidal dipole (TD) modes. The significantly reduced radiation loss of the anapole mode has been employed to enhance SHG efficiency.[34,40] In general, an anapole mode appears as a scattering dip in the scattering spectrum. In Figure 2f, we did not include the TD mode in the decomposition of the scattering spectrum. Although the scattering at ~820 nm involves the contributions of other Mie resonances (e.g., MD and MQ), a scattering dip is still observed if we included the contribution of the TD mode (see the Supporting Information, Figure S6). Therefore, we think that the missing scattering dip in the measured scattering spectrum (Figure 2d) is mainly due to the deviation of the nanoparticle shape from a perfect hexagonal prism. In the numerical simulations, the anapole mode is observed only at $\theta = 0°$ because the formation condition is rather strict. In comparison, the SHG enhancement is also observed at $\theta = 90°$ in the experiments. This is because the femtosecond laser light used to excite the WS_2 nanoparticle is not linearly polarized. We think that the SHG enhancement observed at $\lambda_{ex} \approx 820$ nm is caused by the residual component in the direction $\theta = 0°$. Another difference between the simulated and measured results, which is worth noticing, is the SHG efficiencies of the WGM and the anapole mode. In the simulation results, the SHG efficiency of the WGM at $\theta = 90°$ is larger than that of the anapole mode at $\theta = 0°$. However, we observed reverse behavior in the experiments. The reason is that the WGM is more sensitive to the morphology of the WS_2 nanoparticle, such as the imperfection and roughness, which may dramatically increase the radiation loss of the WGM.

Apart from the SHG enhancement observed at the optical resonances, it is noticed that the SHG intensity exhibits a trend of decreasing with a decreasing wavelength at $\theta = 0°$. In contrast, a reverse behavior is observed at $\theta = 90°$. This feature offers us an opportunity for manipulating the SHG intensity through adjusting the polarization angle of the excitation laser light. In order to show this feature more clearly, we calculated the relative SHG intensities at different wavelengths for the cases of $\theta = 0°$ and $\theta = 90°$, which are defined as follows:

$$I_r(\theta) = \frac{I_{SHG}(\theta)}{\sum I_{SHG}(\theta)}, (\theta = 0°, 90°) \quad (2)$$

The results are listed in Figure 3i. For $\lambda_{ex} < 775$ nm, the relative SHG intensity at $\theta = 0°$ is larger than that at $\theta = 90°$. The situation is reversed when $\lambda_{ex} > 775$ nm. The SHG intensities at $\theta = 0°$ and $\theta = 90°$ become equal at $\lambda_{ex} \approx 775$ nm. Interestingly, this wavelength coincides with the scattering peak of the WS_2 nanoparticle illuminated with unpolarized white light (see Figure 3i). In experiments, we also excited the WS_2 nanoparticle by using femtosecond laser light at $\lambda_{ex} \approx 775$ nm. Surprisingly, it was found that the SHG intensity is

https://doi.org/10.1021/acsanm.3c04844
ACS Appl. Nano Mater. 2024, 7, 726–735

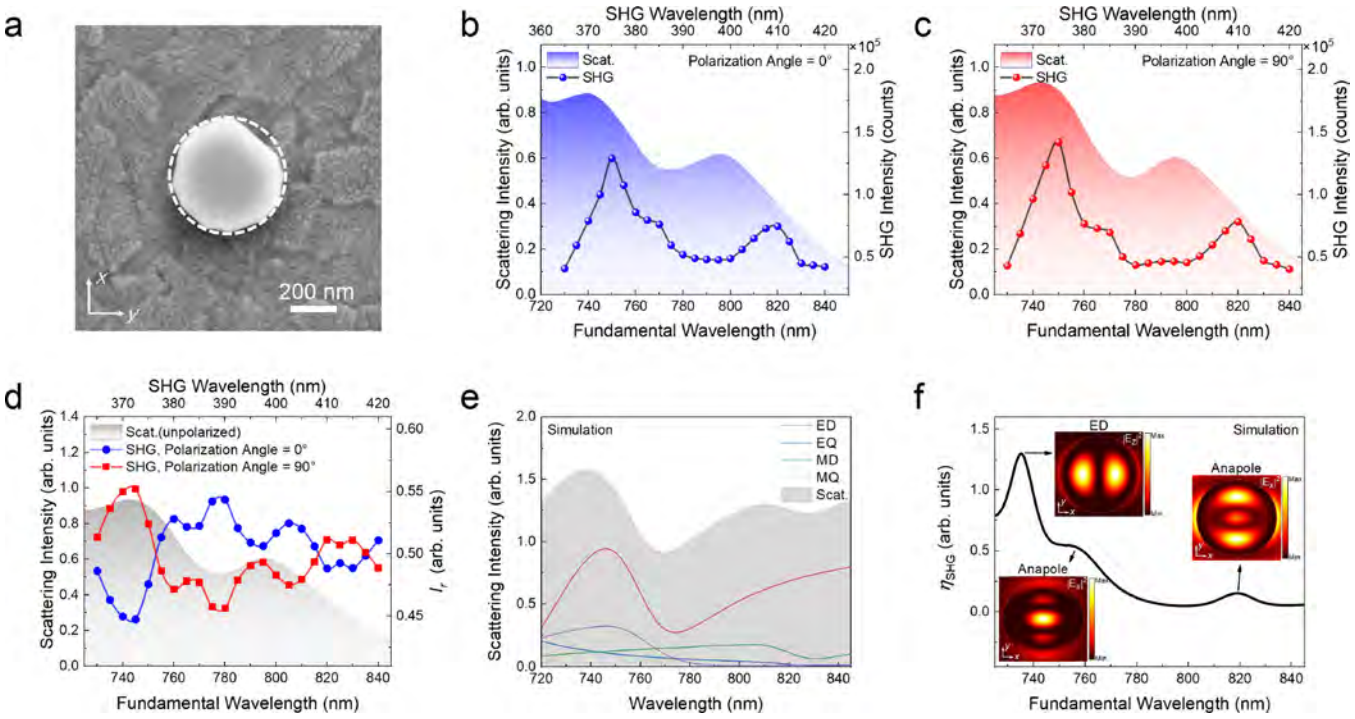

Figure 4. (a) SEM image of a disk-like WS_2 nanoparticle. (b, c) Dependence of the SHG intensity on the excitation wavelength observed for the WS_2 nanodisk at polarization angles of $\theta = 0°$ (a) and $\theta = 90°$. In each case, the scattering spectrum of the WS_2 nanoparticle measured by using white light with the same polarization angle is also provided for reference. (d) Dependence of the relative SHG intensity on the excitation wavelength calculated for the WS_2 nanodisk at polarization angles of $\theta = 0°$ and $\theta = 90°$. The scattering spectrum of the WS_2 nanodisk illuminated with unpolarized white light is provided for reference. (e) Scattering spectrum calculated for the WS_2 nanodisk. The decomposition of the scattering spectrum into Mie resonances is also provided. (f) Dependence of the SHG efficiency on the excitation wavelength simulated for a WS_2 nanodisk with the same dimensions. The electric/magnetic field distributions calculated at different optical resonances are shown as insets.

independent of the polarization angle of the excitation laser light at this wavelength (see the Supporting Information, Figure S7). When the excitation wavelength deviates from this wavelength, the SHG intensity becomes sensitive to the polarization angle of the excitation light, making it possible to manipulate the SHG intensity by simply varying the polarization angle of the excitation light. This intriguing feature is also confirmed in more WS_2 nanoparticles with different morphologies (see the Supporting Information, Figure S8).

Although the SHG in a WS_2 nanoparticle is a second-order nonlinear optical effect, it is closely related to the scattering of the WS_2 nanoparticle, which is a linear optical process. In order to gain deep insight into the relationship between the SHG and the scattering, we simulated the polarization-dependent scattering spectra of this WS_2 nanoparticle (a = 580 nm, b = 444 nm, c = 312 nm, and h = 148 nm), as shown in Figure 3j. It is remarkable that the scattering spectrum is changed dramatically with increasing polarization angle. This behavior is also confirmed by both the numerical simulation and the experimental observation (see the Supporting Information, Figure S9). As discussed above, the scattering of the WS_2 nanoparticle is dominated by the ED mode, which governs the nonlinear optical responses of the WS_2 nanoparticle. We decomposed the scattering spectrum into the contributions of Mie resonances (see the Supporting Information, Figure S10). In Figure 3k, we present the dependence of the ED resonance on the increasing polarization angle. With increasing polarization angle, it was found that the ED resonance is split into two resonances (two peaks). The intensity of the long-wavelength resonance is reduced rapidly, while its wavelength is slightly red-shifted. In contrast, the short-wavelength resonance exhibits a gradual increase in the intensity and a small blue-shift in the wavelength. This behavior explains the wavelength-dependent SHG intensity observed for the two perpendicular angles (Figure 3i). It was revealed that the wavelength at which the SHG intensities at the two polarization angles become equal coincides with the wavelength at which the scattering intensities (or ED amplitudes) at the two polarization angles become equal ($\lambda_{ex} \approx 775$ nm). Therefore, we can conclude that the polarization-dependent SHG intensity observed in such a WS_2 nanoparticle originates from the polarization-dependent ED resonance, which is attributed to the anisotropic geometrical structure of the WS_2 nanoparticle.

In order to explore the impact of the geometrical symmetry of a WS_2 nanoparticle on the SHG of the WS_2 nanoparticle, we intentionally chose a WS_2 nanoparticle with a higher symmetry, which can be considered as a nanodisk, as shown in Figure 4a. The scattering spectra of the WS_2 nanoparticle illuminated with white light polarized along $\theta = 0°$ and $\theta = 90°$ are presented in Figure 4b,c. It was found that the two scattering spectra are quite similar, with two scattering peaks located at $\lambda \approx 750$ and $\lambda \approx 800$ nm. We fixed the polarization angle of the laser light at $\theta = 0°$ or 90° and changed the excitation wavelengths. It was observed that the SHG intensity exhibits a similar dependence on the excitation wavelength, as shown in Figure 4b,c. The enhancement in the SHG intensity is observed at λ_{ex} = 750, 770, and 820 nm. We also calculated the relative SHG intensities at two polarization angles, as shown in Figure 4d. The scattering spectrum of the WS_2

https://doi.org/10.1021/acsanm.3c04844
ACS Appl. Nano Mater. 2024, 7, 726−735

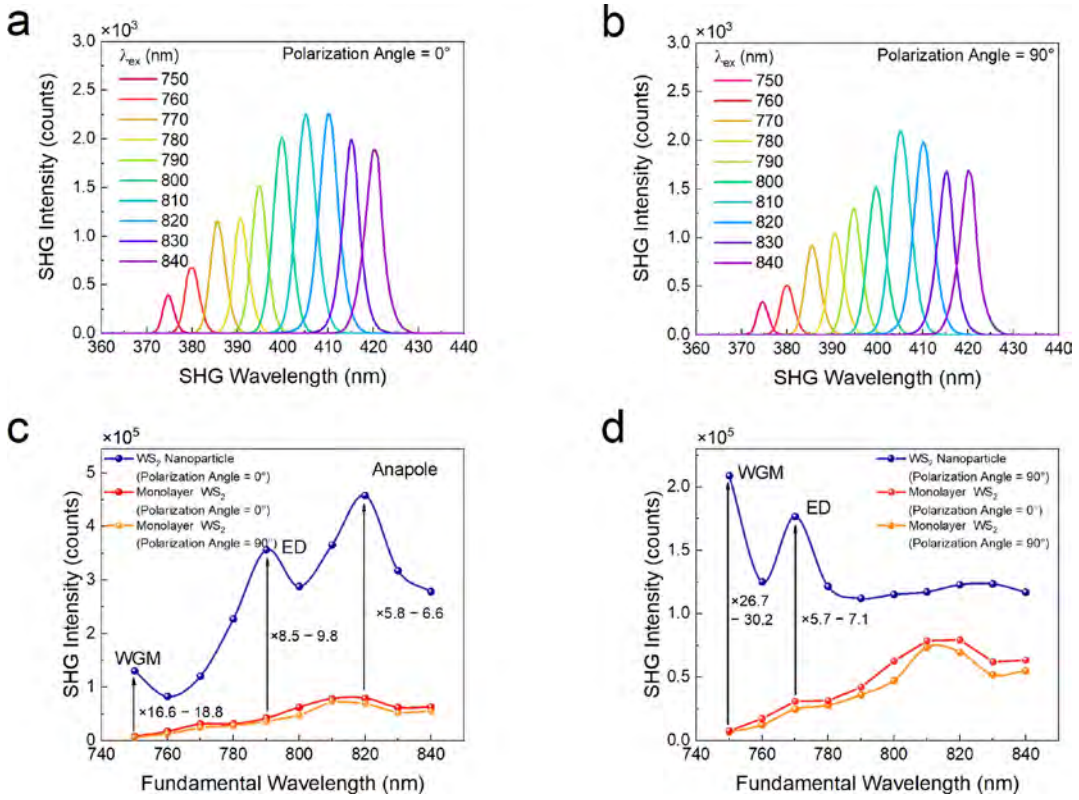

Figure 5. (a, b) SHG spectra measured for a WS_2 monolayer at different excitation wavelengths by using femtosecond laser light polarized along θ = 0° (a) and θ = 90° (b). (c, d) Dependence of the SHG intensity on the excitation wavelength observed for the WS_2 nanoparticle and the WS_2 monolayer at θ = 0° (c) and θ = 90° (d). The enhancement factors observed at different optical resonances are also provided.

nanoparticle illuminated with unpolarized white light is also provided for reference. It was found that the difference between the relative SHG intensities at the two polarization angles becomes smaller. However, the SHG intensity still exhibits polarization dependence at most excitation wavelengths due to the deviation of the nanoparticle shape from that of a perfect nanodisk. In addition, the wavelength at which the relative SHG intensities at two polarization angles become equal does not correspond to the scattering peak. This behavior is different from that observed for the WS_2 nanoparticle with an asymmetric geometry (see Figure 3i). Based on the SEM and AFM observations (see the Supporting Information, Figure S11), we approximated the WS_2 nanoparticle as a nanodisk (r = 227 nm and h = 178 nm) and simulated the scattering spectrum, as shown in Figure 4e. The scattering spectrum is decomposed into Mie resonances of different orders. It can be seen that the scattering is dominated by the ED mode. We also calculated the SHG efficiency of the WS_2 nanodisk based on eq 1, as shown in Figure 4f. The SHG enhancement is observed at three wavelengths (λ_{ex} = 750, 770, and 820 nm), in good agreement with the experimental observations (see Figure 4b,c). The electric field distributions for the three modes exhibiting SHG enhancement are shown in the insets of Figure 4f. Based on the electric field distributions, they are identified as ED and anapole-like modes. For WS_2 nanoparticles with high symmetries (such as nanodisks and hexagonal prisms), one can achieve only SHG enhancement. The manipulation of SHG intensity via the polarization angle of the excitation laser light is not realized (see the Supporting Information, Figures S12 and S13).

Based on the dipole approximation theory, SHG is negligible in bulk materials with centrosymmetry, including WS_2.[6,24] By exploitation of the optical resonances supported by a WS_2 nanoparticle, the SHG of the WS_2 nanoparticle is greatly enhanced. In order to quantitatively evaluate the SHG enhancement, we compared the SHG intensities of a WS_2 nanoparticle and a WS_2 monolayer. Based on previous studies,[25−27] the SHG is observed only in WS_2 with odd layers and the strongest one is found in the WS_2 monolayer. The SHG intensity decreases rapidly with an increasing layer number, and it becomes negligible in bulk WS_2. Therefore, we chose the WS_2 monolayer as reference for the comparison of the SHG intensity. In Figure 5a,b, we present the SHG spectra of the WS_2 monolayer measured for a WS_2 monolayer at different excitation wavelengths by using femtosecond laser light polarized along θ = 0° and 90°, respectively. It is noticed that the SHG of the WS_2 monolayer exhibits a similar dependence on the excitation wavelength for the two polarization angles. A detailed examination reveals that the maximum SHG intensity appears at θ = 0° while the minimum one appears at θ = 90° (see the Supporting Information, Figure S14). In Figure 5c,d, we compared the SHG intensities of the WS_2 nanoparticle and WS_2 monolayer under the same excitation conditions for θ = 0° and 90°. In both cases, the SHG intensity of the WS_2 nanoparticle is much larger than that of the WS_2 monolayer, especially at optical resonances (e.g., ED, WGM, and anapole). The enhancement factor for the SHG intensity can be as large as ∼30. The large enhancement in combination with the manipulation ability implies the potential applications of WS_2 nanoparticles in the construction of nanoscale nonlinear optical devices.

https://doi.org/10.1021/acsanm.3c04844
ACS Appl. Nano Mater. 2024, 7, 726−735

CONCLUSIONS

In summary, we have investigated systematically the SHG in WS_2 nanoparticles with different symmetries. It was found that the SHG can be dramatically enhanced at optical resonances supported by WS_2 nanoparticles, such as ED, WGM, and anapole resonances. It was revealed that the SHG enhancement exhibits a strong dependence on the polarization of the excitation light in WS_2 nanoparticles with lower symmetries, which offers us an opportunity to manipulate the SHG intensity by simply varying the polarization angle. This feature is manifested in the polarization-dependent scattering of WS_2 nanoparticles because the SHG enhancement is dominated mainly by the ED resonance. It was shown that the SHG intensity from a WS_2 nanoparticle is much larger than that from a WS_2 monolayer, with an enhancement factor of up to ~30. Our findings are helpful for understanding the physical mechanism for the SHG in centrosymmetric materials and useful for designing nanoscale nonlinear optical devices based on TMDC nanoparticles.

METHODS

Sample Fabrication. The WS_2 nanoparticles and WS_2 monolayers used in this work were purchased from Sixcarbon Tech Shenzhen. The WS_2 nanoparticles used in this study were synthesized by using the chemical vapor deposition method. First, W and S were mixed at a molar ratio of 1:2 and sealed in a quartz tube with high vacuum. Then, the mixture was heated to 900 °C and kept at this temperature for 100 h. The WS_2 powder obtained in this way was dispersed uniformly in deionized water by using an ultrasonic wave. After that, the aqueous solution containing WS_2 nanoparticles was separated by centrifugation, dropped on an ITO substrate, and dried naturally. Based on the SEM observation, the WS_2 nanoparticles obtained in this way may exhibit different morphologies and sizes (see the Supporting Information, Figure S2). It was easy to find hexagonal-prism-like WS_2 nanoparticles because it is a relatively stable structure for WS_2. Based on the electron diffraction pattern and X-ray diffraction spectrum, the crystal structure of the WS_2 nanoparticles is dominated by the 2H phase (see the Supporting Information, Figures S15 and S16 and Table S1).

Optical Characterization. The linear and nonlinear optical responses of WS_2 nanoparticles were characterized by using an inverted microscope (Observer A1, Zeiss) equipped with white light and a femtosecond laser as excitation sources.

The scattering properties of WS_2 nanoparticles were characterized by using a dark-field microscope with a home-built oblique incidence system. In this case, the illumination light is incident on the WS_2 nanoparticles at an angle of approximately 40°, and the forward scattered light is collected by the objective lens of the dark-field microscope.

WS_2 nanoparticles and monolayers were excited by using focused femtosecond laser light with a 100× objective lens. The polarization of the femtosecond laser light was changed by using a home-built polarizer. The SHG intensities from WS_2 nanoparticles and monolayers were collected by using the same objective and directed to a spectrometer (SR-500i-B1, Andor) for spectral analysis or charge coupled devices (DU970N, Andor) for imaging.

ASSOCIATED CONTENT

Supporting Information

The Supporting Information is available free of charge at https://pubs.acs.org/doi/10.1021/acsanm.3c04844.

Simulated scattering spectra for a WS_2 nanoparticle placed on a silica (SiO_2) substrate without and with a thin ITO film; morphology characterization of WS_2 nanoparticles; SEM images and scattering spectra of more WS_2 nanoparticles; height characterization of WS_2 nanoparticles; dependence of the SHG intensity of a WS_2 nanoparticle on the pumping power; multipolar decomposition of the scattering spectrum of a WS_2 nanoparticle; dependence of the SHG intensity of a WS_2 nanoparticle on the polarization angle of the excitation laser light; polarization-dependent SHG intensity observed in more WS_2 nanoparticles; evolution of the scattering spectrum with increasing polarization angle and multipole decomposition of the scattering spectrum for a hexagonal-prism-like WS_2 nanoparticle; height characterization of WS_2 nanoparticles; polarization-dependent scattering spectra simulated for a hexagonal-prism WS_2 nanoparticle; electric and magnetic field distributions calculated at the optical resonances supported by a hexagonal-prism WS_2 nanoparticle; dependence of the SHG intensity on the polarization angle observed for a WS_2 monolayer; analysis of the crystal structure of WS_2 (PDF)

AUTHOR INFORMATION

Corresponding Author

Sheng Lan − *Guangdong Provincial Key Laboratory of Nanophotonic Functional Materials and Devices, School of Information and Optoelectronic Science and Engineering, South China Normal University, Guangzhou 510006, China;* orcid.org/0000-0002-7277-0042; Email: slan@scnu.edu.cn

Authors

Tianxiang Yu − *Guangdong Provincial Key Laboratory of Nanophotonic Functional Materials and Devices, School of Information and Optoelectronic Science and Engineering, South China Normal University, Guangzhou 510006, China;* orcid.org/0009-0006-0626-5896

Mingcheng Panmai − *School of Electrical and Electronic Engineering, Nanyang Technological University, 639798, Singapore*

Shulei Li − *School of Optoelectronic Engineering, Guangdong Polytechnic Normal University, Guangzhou 510665, China*

Shimei Liu − *Guangdong Provincial Key Laboratory of Nanophotonic Functional Materials and Devices, School of Information and Optoelectronic Science and Engineering, South China Normal University, Guangzhou 510006, China;* orcid.org/0000-0001-5704-095X

Yuheng Mao − *Guangdong Provincial Key Laboratory of Nanophotonic Functional Materials and Devices, School of Information and Optoelectronic Science and Engineering, South China Normal University, Guangzhou 510006, China;* orcid.org/0009-0007-6267-7120

Lidan Zhou − *State Key Laboratory of Optoelectronic Materials and Technologies, School of Electronics and Information Technology, Sun Yat-sen University, Guangzhou 51006, China;* orcid.org/0000-0003-3146-9082

Complete contact information is available at: https://pubs.acs.org/10.1021/acsanm.3c04844

Author Contributions

#T.Y. and M.P. contributed equally to this work. S.L., T.Y., and M.P. conceived the idea. T.Y. performed the numerical simulations. M.P., T.Y., and Y.M. carried out the optical measurements. S.L., T.Y., M.P., S.L., S.L., and L.Z. analyzed the

https://doi.org/10.1021/acsanm.3c04844
ACS Appl. Nano Mater. 2024, 7, 726−735

data and wrote the manuscript. S. Lan supervised the project. All the authors read and commented on the manuscript.

Notes

The authors declare no competing financial interest.

■ ACKNOWLEDGMENTS

S. Lan acknowledges the financial support from the National Natural Science Foundation of China (grant nos. 12174123 and 12374347). S. Li acknowledges the financial support from the Natural Science Foundation of Guangdong Province, China (grant no. 2022A1515010747).

■ REFERENCES

(1) Pu, Y.; Grange, R.; Hsieh, C.-L.; Psaltis, D. Nonlinear Optical Properties of Core-Shell Nanocavities for Enhanced Second-Harmonic Generation. *Phys. Rev. Lett.* **2010**, *104*, No. 207402.

(2) Ji, L.; Zhao, X.; Liu, D.; Gao, Y.; Cui, Y.; Rao, D.; Feng, W.; Li, F.; Shi, H.; Liu, J.; Li, X.; Xia, L.; Wang, T.; Liu, J.; Du, P.; Sun, X.; Ma, W.; Sui, Z.; Chen, X. High-Efficiency Second-Harmonic Generation of Low-Temporal-Coherent Light Pulse. *Opt. Lett.* **2019**, *44*, 4359−4362.

(3) Mushtaq, A.; Clink, L.; Noor, M. Y.; Kuz, C.; DeAngelis, E.; Siebenaller, R.; Fisher, A.; Verma, D.; Myers, R. C.; Conner, B. S.; Susner, M. A.; Chowdhury, E. Ultrafast Nonlinear Absorption and Second Harmonic Generation in $Cu_{0.33}In_{1.30}P_2S_6$ Van Der Waals Layered Crystals. *J. Phys. Chem. Lett.* **2022**, *13*, 10513−10521.

(4) Tran, R. J.; Sly, K. L.; Conboy, J. C. Applications of Surface Second Harmonic Generation in Biological Sensing. *Annu. Rev. Anal. Chem.* **2017**, *10*, 387−414.

(5) Bhalla, P.; Das, K.; Culcer, D.; Agarwal, A. Resonant Second-Harmonic Generation as a Probe of Quantum Geometry. *Phys. Rev. Lett.* **2022**, *129*, No. 227401.

(6) Liu, H.; Li, Y.; You, Y. S.; Ghimire, S.; Heinz, T. F.; Reis, D. A. High-Harmonic Generation from an Atomically Thin Semiconductor. *Nat. Phys.* **2017**, *13*, 262−265.

(7) Kauranen, M.; Zayats, A. V. Nonlinear Plasmonics. *Nat. Photonics* **2012**, *6*, 737−748.

(8) Smirnova, D.; Kivshar, Y. S. Multipolar Nonlinear Nanophotonics. *Optica* **2016**, *3*, 1241−1255.

(9) Husu, H.; Siikanen, R.; Mäkitalo, J.; Lehtolahti, J.; Laukkanen, J.; Kuittinen, M.; Kauranen, M. Metamaterials with Tailored Nonlinear Optical Response. *Nano Lett.* **2012**, *12*, 673−677.

(10) Mobini, E.; Alaee, R.; Boyd, R. W.; Dolgaleva, K. Giant Asymmetric Second-Harmonic Generation in Bianisotropic Metasurfaces Based on Bound States in the Continuum. *ACS Photonics* **2021**, *8*, 3234−3240.

(11) Makarov, S. V.; Petrov, M. I.; Zywietz, U.; Milichko, V.; Zuev, D.; Lopanitsyna, N.; Kuksin, A.; Mukhin, I.; Zograf, G.; Ubyivovk, E.; Smirnova, D. A.; Starikov, S.; Chichkov, B. N.; Kivshar, Y. S. Efficient Second-Harmonic Generation in Nanocrystalline Silicon Nanoparticles. *Nano Lett.* **2017**, *17*, 3047−3053.

(12) Timofeeva, M.; Lang, L.; Timpu, F.; Renaut, C.; Bouravleuv, A.; Shtrom, I.; Cirlin, G.; Grange, R. Anapoles in Free-Standing Iii−V Nanodisks Enhancing Second-Harmonic Generation. *Nano Lett.* **2018**, *18*, 3695−3702.

(13) Turquet, L.; Kakko, J.; Zang, X.; Naskali, L.; Karvonen, L.; Jiang, H.; Huhtio, T.; Kauppinen, E.; Lipsanen, H.; Kauranen, M.; Bautista, G. Tailorable Second-Harmonic Generation from an Individual Nanowire Using Spatially Phase-Shaped Beams. *Laser Photon. Rev.* **2017**, *11*, 1600175.

(14) Liu, S.; Sinclair, M. B.; Saravi, S.; Keeler, G. A.; Yang, Y.; Reno, J.; Peake, G. M.; Setzpfandt, F.; Staude, I.; Pertsch, T.; Brener, I. Resonantly Enhanced Second-Harmonic Generation Using Iii−V Semiconductor All-Dielectric Metasurfaces. *Nano Lett.* **2016**, *16*, 5426−5432.

(15) Koshelev, K.; Kruk, S.; Melik-Gaykazyan, E.; Choi, J.-H.; Bogdanov, A.; Park, H.-G.; Kivshar, Y. J. S. Subwavelength Dielectric Resonators for Nonlinear Nanophotonics. *Science* **2020**, *367*, 288−292.

(16) Kroychuk, M. K.; Yagudin, D. F.; Shorokhov, A. S.; Smirnova, D. A.; Volkovskaya, I. I.; Shcherbakov, M. R.; Shvets, G.; Kivshar, Y. S.; Fedyanin, A. A. Tailored Nonlinear Anisotropy in Mie-Resonant Dielectric Oligomers. *Adv. Opt. Mater.* **2019**, *7*, 1900447.

(17) Ermolaev, G. A.; Grudinin, D. V.; Stebunov, Y. V.; Voronin, K. V.; Kravets, V. G.; Duan, J.; Mazitov, A. B.; Tselikov, G. I.; Bylinkin, A.; Yakubovsky, D. I.; Novikov, S. M.; Baranov, D. G.; Nikitin, A. Y.; Kruglov, I. A.; Shegai, T.; Alonso-González, P.; Grigorenko, A. N.; Arsenin, A. V.; Novoselov, K. S.; Volkov, V. S. Giant Optical Anisotropy in Transition Metal Dichalcogenides for Next-Generation Photonics. *Nat. Commun.* **2021**, *12*, 854.

(18) Li, Y.; Chernikov, A.; Zhang, X.; Rigosi, A.; Hill, H. M.; van der Zande, A. M.; Chenet, D. A.; Shih, E.-M.; Hone, J.; Heinz, T. F. Measurement of the Optical Dielectric Function of Monolayer Transition-Metal Dichalcogenides: MoS_2,$MoSe_2$,WS_2,and WSe_2. *Phys. Rev. B* **2014**, *90*, No. 205422.

(19) Green, T. D.; Baranov, D. G.; Munkhbat, B.; Verre, R.; Shegai, T.; Käll, M. Optical Material Anisotropy in High-Index Transition Metal Dichalcogenide Mie Nanoresonators. *Optica* **2020**, *7*, 680−686.

(20) Qiu, D. Y.; da Jornada, F. H.; Louie, S. G. Optical Spectrum of MoS_2: Many-Body Effects and Diversity of Exciton States. *Phys. Rev. Lett.* **2013**, *111*, No. 216805.

(21) Mak, K. F.; Shan, J. Photonics and Optoelectronics of 2d Semiconductor Transition Metal Dichalcogenides. *Nat. Photonics* **2016**, *10*, 216−226.

(22) Ermolaev, G. A.; Yakubovsky, D. I.; Stebunov, Y. V.; Arsenin, A. V.; Volkov, V. S. Spectral Ellipsometry of Monolayer Transition Metal Dichalcogenides: Analysis of Excitonic Peaks in Dispersion. *J. Vac. Sci. Technol., B: Nanotechnol. Microelectron.: Mater., Process., Meas., Phenom.* **2020**, *38*, No. 014002.

(23) Anantharaman, S. B.; Jo, K.; Jariwala, D. Exciton−Photonics: From Fundamental Science to Applications. *ACS Nano* **2021**, *15*, 12628−12654.

(24) Popkova, A. A.; Antropov, I. M.; Tselikov, G. I.; Ermolaev, G. A.; Ozerov, I.; Kirtaev, R. V.; Novikov, S. M.; Evlyukhin, A. B.; Arsenin, A. V.; Bessonov, V. O.; Volkov, V. S.; Fedyanin, A. A. Nonlinear Exciton-Mie Coupling in Transition Metal Dichalcogenide Nanoresonators. *Laser Photon. Rev.* **2022**, *16*, 2100604.

(25) Malard, L. M.; Alencar, T. V.; Barboza, A. P. M.; Mak, K. F.; De Paula, A. M. J. P. R. B. Observation of Intense Second Harmonic Generation from MoS_2 Atomic Crystals. *Phys. Rev. B* **2013**, *87*, No. 201401.

(26) Säynätjoki, A.; Karvonen, L.; Rostami, H.; Autere, A.; Mehravar, S.; Lombardo, A.; Norwood, R. A.; Hasan, T.; Peyghambarian, N.; Lipsanen, H.; Kieu, K.; Ferrari, A. C.; Polini, M.; Sun, Z. Ultra-Strong Nonlinear Optical Processes and Trigonal Warping in MoS_2 Layers. *Nat. Commun.* **2017**, *8*, 893.

(27) Kumar, N.; Najmaei, S.; Cui, Q.; Ceballos, F.; Ajayan, P. M.; Lou, J.; Zhao, H. Second Harmonic Microscopy of Monolayer MoS_2. *Phys. Rev. B* **2013**, *87*, No. 161403.

(28) Hu, G.; Hong, X.; Wang, K.; Wu, J.; Xu, H.-X.; Zhao, W.; Liu, W.; Zhang, S.; Garcia-Vidal, F.; Wang, B.; Lu, P.; Qiu, C.-W. Coherent Steering of Nonlinear Chiral Valley Photons with a Synthetic Au−WS_2 Metasurface. *Nat. Photonics* **2019**, *13*, 467−472.

(29) Wang, Z.; Dong, Z.; Zhu, H.; Jin, L.; Chiu, M.-H.; Li, L.-J.; Xu, Q.-H.; Eda, G.; Maier, S. A.; Wee, A. T. S.; Qiu, C.-W.; Yang, J. K. W. Selectively Plasmon-Enhanced Second-Harmonic Generation from Monolayer Tungsten Diselenide on Flexible Substrates. *ACS Nano* **2018**, *12*, 1859−1867.

(30) Duong, N. M. H.; Xu, Z.-Q.; Kianinia, M.; Su, R.; Liu, Z.; Kim, S.; Bradac, C.; Tran, T. T.; Wan, Y.; Li, L.-J.; Solntsev, A.; Liu, J.; Aharonovich, I. Enhanced Emission from WSe_2 Monolayers Coupled to Circular Bragg Gratings. *ACS Photonics* **2018**, *5*, 3950−3955.

(31) Yi, F.; Ren, M.; Reed, J. C.; Zhu, H.; Hou, J.; Naylor, C. H.; Johnson, A. T. C.; Agarwal, R.; Cubukcu, E. Optomechanical Enhancement of Doubly Resonant 2d Optical Nonlinearity. *Nano Lett.* **2016**, *16*, 1631−1636.

https://doi.org/10.1021/acsanm.3c04844
ACS Appl. Nano Mater. 2024, 7, 726−735

(32) Shi, J.; Wu, X.; Wu, K.; Zhang, S.; Sui, X.; Du, W.; Yue, S.; Liang, Y.; Jiang, C.; Wang, Z.; Wang, W.; Liu, L.; Wu, B.; Zhang, Q.; Huang, Y.; Qiu, C.-W.; Liu, X. Giant Enhancement and Directional Second Harmonic Emission from Monolayer WS_2 on Silicon Substrate Via Fabry-Pérot Micro-Cavity. *ACS Nano* **2022**, *16*, 13933−13941.
(33) Sortino, L.; Zotev, P. G.; Mignuzzi, S.; Cambiasso, J.; Schmidt, D.; Genco, A.; Aßmann, M.; Bayer, M.; Maier, S. A.; Sapienza, R.; Tartakovskii, A. I. Enhanced Light-Matter Interaction in an Atomically Thin Semiconductor Coupled with Dielectric Nano-Antennas. *Nat. Commun.* **2019**, *10*, 5119.
(34) Busschaert, S.; Reimann, R.; Cavigelli, M.; Khelifa, R.; Jain, A.; Novotny, L. Transition Metal Dichalcogenide Resonators for Second Harmonic Signal Enhancement. *ACS Photonics* **2020**, *7*, 2482−2488.
(35) Sung, J.; Shin, D.; Cho, H.; Lee, S. W.; Park, S.; Kim, Y. D.; Moon, J. S.; Kim, J.-H.; Gong, S.-H. Room-Temperature Continuous-Wave Indirect-Bandgap Transition Lasing in an Ultra-Thin WS_2 Disk. *Nat. Photonics* **2022**, *16*, 792−797.
(36) Nauman, M.; Yan, J.; de Ceglia, D.; Rahmani, M.; Zangeneh Kamali, K.; De Angelis, C.; Miroshnichenko, A. E.; Lu, Y.; Neshev, D. N. Tunable Unidirectional Nonlinear Emission from Transition-Metal-Dichalcogenide Metasurfaces. *Nat. Commun.* **2021**, *12*, 5597.
(37) Muhammad, N.; Chen, Y.; Qiu, C.-W.; Wang, G. P. Optical Bound States in Continuum in MoS_2-Based Metasurface for Directional Light Emission. *Nano Lett.* **2021**, *21*, 967−972.
(38) Munkhbat, B.; Wróbel, P.; Antosiewicz, T. J.; Shegai, T. O. Optical Constants of Several Multilayer Transition Metal Dichalcogenides Measured by Spectroscopic Ellipsometry in the 300−1700 Nm Range: High Index, Anisotropy, and Hyperbolicity. *ACS Photonics* **2022**, *9*, 2398−2407.
(39) Verre, R.; Baranov, D. G.; Munkhbat, B.; Cuadra, J.; Käll, M.; Shegai, T. Transition Metal Dichalcogenide Nanodisks as High-Index Dielectric Mie Nanoresonators. *Nat. Nanotechnol.* **2019**, *14*, 679−683.
(40) Miroshnichenko, A. E.; Evlyukhin, A. B.; Yu, Y. F.; Bakker, R. M.; Chipouline, A.; Kuznetsov, A. I.; Luk'yanchuk, B.; Chichkov, B. N.; Kivshar, Y. S. Nonradiating Anapole Modes in Dielectric Nanoparticles. *Nat. Commun.* **2015**, *6*, 8069.

https://doi.org/10.1021/acsanm.3c04844
ACS Appl. Nano Mater. 2024, 7, 726−735